Astron. Astrophys. 186, 64–76 (1987)

ASTRONOMY
AND
ASTROPHYSICS

Star formation in the nucleus of the galaxy NGC 5253*

R. González-Riestra [1], M. Rego [2], and J. Zamorano [2]

[1] IUE Observatory, European Space Agency, P.O. Box 54065, E-28080 Madrid, Spain
[2] Departamento de Astrofísica, Facultad de Ciencias Físicas, Universidad Complutense, E-28040 Madrid, Spain

Received February 11, accepted May 11, 1987

Summary. Optical and ultraviolet spectroscopic observations of the nucleus of the galaxy NGC 5253 are analyzed. This galaxy presents the typical features of an elliptical system at large distances from its center. However, its nucleus is dominated by an emission complex composed by several giant H II regions. The analysis of the optical spectra shows that the metallic abundances in the nucleus of the galaxy are below the solar values. The presence of O stars can be deduced from the numerous absorption lines present in the UV spectrum. The UV emission lines indicate a high effective temperature for the ionizing star cluster. The comparison of the observations with evolutive models of $W(H\beta)$ and the slope of the UV continuum shows that the age of the brightest knot of the nucleus of NGC 5253 is less than three millions years. The exact age depends on the choice of the extinction law, not well known in this type of objects. An LMC-like law (consistent with the low metallicity of the object) leads to an age of 2.3 10^6 yr, and to an IMF similar or slightly flatter than that found by Salpeter for the solar neighbourhood, with an upper mass limit in the range $60\,M_\odot < M_{up} < 120\,M_\odot$.

Key words: extragalactic H II regions – star formation – initial mass function – UV radiation

1. Introduction

The southern galaxy NGC 5253 has been the object of many studies due to the noticeable characteristics of its nucleus. This galaxy is classified as "Irregular non Magellanic and Peculiar" in the Second Reference Catalog of Bright Galaxies (de Vaucouleurs et al., 1976). Sandage and Brucato (1979) included it in the class of Amorphous galaxies. The distribution of surface brigthness in the outer regions ($r > 30''$) is similar to that found in elliptical galaxies (Welch, 1970). The characteristics derived from the Hydrogen 21 cm (Bottinelli et al., 1972) place it between early-type galaxies as well.

However, the nuclear zone of NGC 5253 exhibits a spectrum with a very blue continuum and emission lines superposed, similar to that found in galactic and extragalactic H II regions (Evans, 1956; Burbidge and Burbidge, 1962; Welch and Wallerstein, 1968; Welch, 1970; Sersic et al., 1972; Bohuski et al., 1972; Osmer et al., 1974; Hunter et al., 1982).

In the nucleus of NGC 5253 there are several bright knots that can be identified as clusters of young stars or H II regions (Sersic et al., 1972; Hunter, 1982) and some dust patches. The existence of such features suggests that a strong burst of star formation has taken place recently in the center of this galaxy. The very blue optical colors (e.g. Veron, 1984), the infrared studies (Aitken et al., 1982; Moorwood and Glass, 1982; Campbell and Terlevich, 1984), and the high rate of type I supernovae (two in one century: SN 1895 B and SN 1972 E) support this conclusion.

Van den Bergh (1972, 1980) has pointed out the existence of a large number of star-like objects surrounding the center of the galaxy, that he identifies as clusters of young stars. They show an absorption spectrum typical of early-type stars with an emission line spectrum superposed. This author suggests that the cause that triggered the burst of star formation was a close encounter with the nearby spiral galaxy M 83. These clusters would indicate that in the past ($1\ 10^8 - 1\ 10^9$ yr ago) the star formation extended along all the galaxy, being now confined to the nucleus. Table 1 gives the general characteristics of NGC 5253.

2. Observations

2.1. Optical observations

The observations were performed with the 3.6-m. Telescope at the European Southern Observatory (ESO) La Silla (Chile) during the night 1978 Sept 9–10 by Dr. W. Wamsteker with the Intensified Photon Counting System (IPCS) (Boksenberg, 1972) and the Bollers and Chivens spectrograph. The wavelength range covered extended from 3600 to 6800 Å at a dispersion of 114 Å/mm. The slit was oriented along the position angle P.A. = 240°. Three images of NGC 5253 were obtained, with slit widths of 3″, 0.″4 and 0.″2 respectively to avoid the saturation of the spectra in the strongest emission lines; only at a slit width of 0.″2 no lines were saturated. The format of the images was 1500 pixels by 70 spatial increments, of 1.″76 on the sky.

The data were reduced with the ESO-IHAP system (Middelburg and Crane, 1979) at the Villafranca Tracking Station (ESA, Madrid). The standard procedure followed includes flat-fielding, wavelength calibration, atmospheric extinction correction by means of the standard extinction curve for La Silla, and calibration in absolute fluxes using observations of white dwarfs standards (Oke, 1974). The journal of the observations is presented in Table 2.

Send offprint requests to: R. González-Riestra

* Based on observations collected at the European Southern Observatory (La Silla, Chile), and in data from the International Ultraviolet Explorer dearchived from the Villafranca Data Archive of the European Space Agency

Table 1. General Properties of NGC5253

$\alpha(1950.0) = 13^h57^m09^s$	de Vaucouleurs et al. (1976)
$\delta(1950.0) = -21°23'24''$	de Vaucouleurs et al. (1976)
$B_T^\circ = 10.37$	de Vaucouleurs et al. (1976)
Morph. type: Irregular Non Magellanic and Peculiar.	de Vaucouleurs et al. (1976)
Amorphous.	Sandage and Tamman (1981)
$D = 4$ Mpc	Bottinelli et al. (1972)
$M(\mathrm{H\,I}) = 0.18\ 10^9 M_\odot$	Bottinelli et al. (1972)
$0.39\ 10^9 M_\odot$	Lewis and Davis (1972)
$0.17\ 10^9 M_\odot$	Reif et al. (1982)
v [a] = 197 km/s (radio)	Bottinelli et al. (1972)
199 km/s (radio)	Lewis and Davis (1972)
227 km/s (radio)	Reif et al. (1982)
208 km/s (optical)	Welch (1970)
213 km/s (optical)	Bohuski et al. (1972)
214 km/s (optical)	Sersic et al. (1972)
$B-V = 0.22$	Wegner (1979)
$U-B = -0.66$	Wegner (1979) Aperture = 10".5
$J-H = 0.78$	Campbell and Terlevich (1984)
$H-K = 0.16$	Campbell and Terlevich (1984) Aperture = 5"
$L_x = 3\ 10^{38}$ erg s^{-1}	Moorwood and Glass (1982)
$L(\mathrm{H}\beta) = 8.5\ 10^{39}$ erg/s^{-1}	Osmer et al. (1974)
$7.9\ 10^{39}$ erg/s^{-1}	Terlevich and Melnick (1981)
$9.1\ 10^{39}$ erg/s^{-1}	Hunter et al. (1982)

[a] Velocity corrected for solar motion

Table 2. Journal of optical observations

Image	PA	Slit	T_{exp} (min)	Comments
No. 1	240	3"	24.5	Hβ and [O III] saturated
No. 2	240	0".4	13.5	[O III] saturated
No. 3	240	0".2	4.5	

Ultraviolet data

Image	PA	T_{exp} (min)	Comments
SWP 13484	27	200	Continuum >150 DN above background
LWR 3131	166	105	Continuum >150 DN above background

As we have pointed out above, only one of our images (No. 3) does not show saturation in the [O III] $\lambda\lambda$4959, 5007 emission lines. For this reason all the line measurements reported here have been carried out in image No. 2, except the [O III]/Hβ ratio which has been measured in image No. 3.

The position angle of the slit was chosen to allow the simultaneous observation of the principal knots of the nucleus of the galaxy. A detailed description of the morphology of the center of NGC5253 has been given by other authors (e.g. Welch, 1970; Sersic et al., 1972; Hunter, 1982). Hα images of the nucleus of NGC5253 show an emission complex that extends over a region of 30" × 15". Inside this complex there is a bright condensation of about 6" diameter – hereafter, nucleus (a) – and to the South several knots less bright and smaller than the first one. The second brightest condensation (nucleus (b)) is 6"–8" apart from the first one along the position angle 240°. In Fig. 1 we present a scheme of the nucleus of NGC5253, adapted from Sersic et al. (1972), where the different knots and the slit position and orientation are shown.

The first image (No. 1), having been taken with the widest slit and the longest exposure time, was chosen to study the distribution of the continuum radiation along the slit. The band between 5100 and 5150 Å has been chosen because, being free of strong emission lines, its distribution represents that of the stars. In Fig. 2 we represent the star emission distribution. Along with the principal maximum that marks the position of nucleus (a), another secondary maximum can be seen placed ~7" Southwest

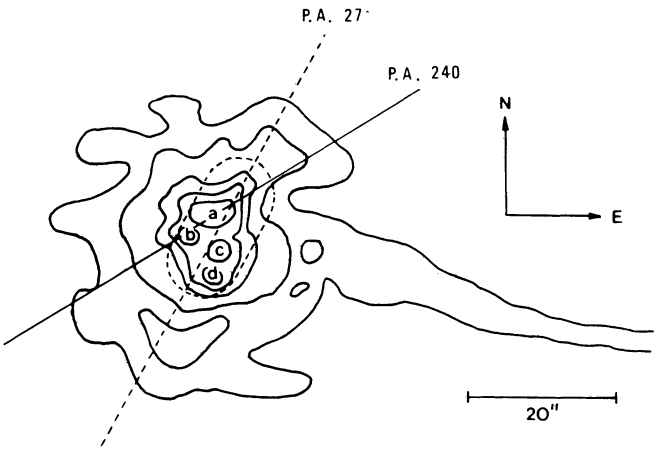

Fig. 1. Morphology of the nucleus of NGC5253 (Sersic et al., 1972). The solid line shows the position of the slit used in the IPCS observations. The broken line marks the position of the IUE slit in the short-wavelength spectrum described in the text

of the first one. By comparing this Fig. 2 to Fig. 1 this second maximum can be easily identified with knot (b).

Special mention must be done to another emission region located well outside the nuclear zone, $\sim 25''$ to the North of the main nucleus (see Fig. 2). Its spectrum show a red continuum which a few emission lines superposed (strong 3727, weak 4959, 5007, and even weaker Hβ, Hα and possibly [N II]). The signal-to-noise ratio, even in the best-exposed image does not allow a detailed study of this spectrum, but its redness is indicative of the presence of a relatively old stellar population.

In Fig. 3 we show the variation of the intensities of the lines [O II] λ3727, Hβ and [O III] λ5007, representative of the distribution of the ionized gas. The Oxygen lines, both λ3727 and λ5007 have been detected in a region of a radius of 30″ around nucleus (a), and Hβ in a slightly smaller area of 25″ of radius.

Figure 4 shows the sky-substracted spectrum of the nucleus of NGC5253. This spectrum has been obtained by adding the signal in the spatial increments where emission lines have been detected (i.e. $\sim 1'$ or 1.2 kpc if a distance of 4 Mpc is assumed).

The radial velocity, measured from the emission lines is 368 ± 32 km s^{-1}. The corresponding value corrected for the Earth and solar motions reduces to 206 ± 32 km s^{-1}, in agreement with previous results obtained from optical and radio measurements (see Table 1).

The intensities of the emission lines were obtained by fitting them to gaussian functions. In the case of blending ([S II] $\lambda\lambda$6717, 6731, [N II] $\lambda\lambda$6548, 6584 + Hα) a gaussian deblending was used.

The color excess was determined assuming that the Hydrogen lines arise only from case B recombination and fitting the observed Hα/Hβ ratio to the one computed by Brocklehurst (1971) for $T_e = 15000$ K and $N_e = 100$ cm^{-3}. Higher members of the Balmer serie have not been used because of their weakness and a possible underlying stellar absorption. The measured Hα/Hβ ratio of 4.32 leads to a color excess of $E(B-V) = 0.41$, assuming a standard galactic reddening law as given by Osterbrock (1974). The Hydrogen maps of Burstein and Heiles (1984) indicate only $E(B-V) = 0.04$ of galactic foreground reddening in this direction. Therefore most of the observed galactic reddening must be internal to NGC5253.

In Table 3 we present the measured ($I(\lambda)$) and reddening corrected ($F(\lambda)$) intensities of the emission lines scaled to $I(\mathrm{H}\beta) = 100$.

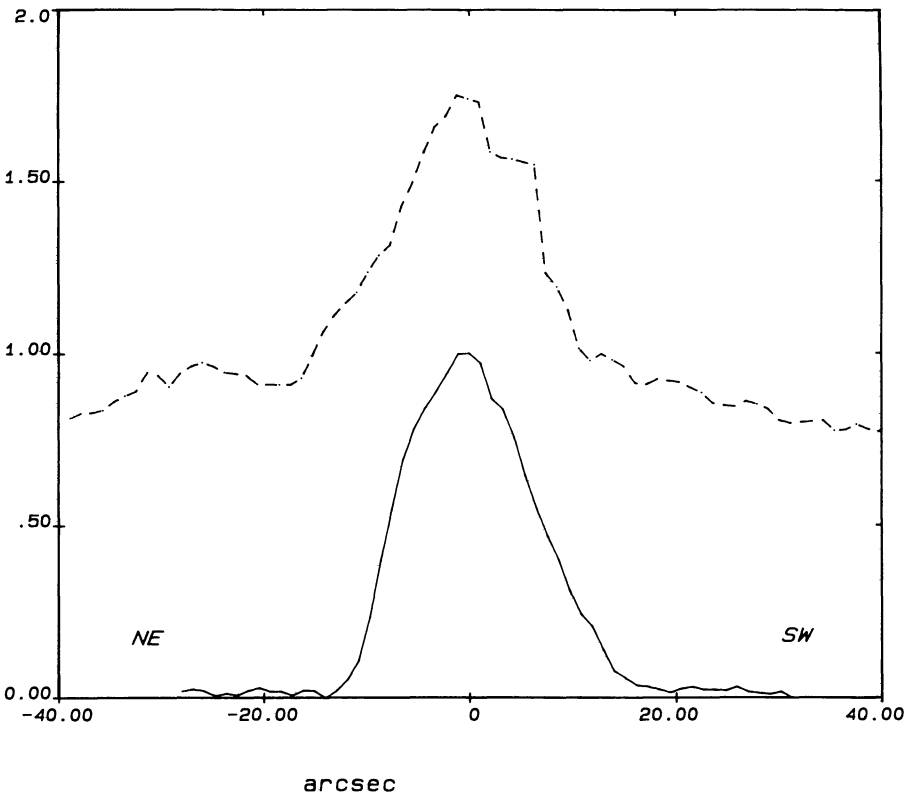

Fig. 2. Spatial distribution of the intensity in two bands of continuum: Solid line: 1300–1400 Å along PA 27°; Dashed line: 5100–5150 Å along PA 240°. The values are normalized to 1 in the point of maximum intensity. An offset of 0.75 units has been added to the optical profile in order to make the figure clearer

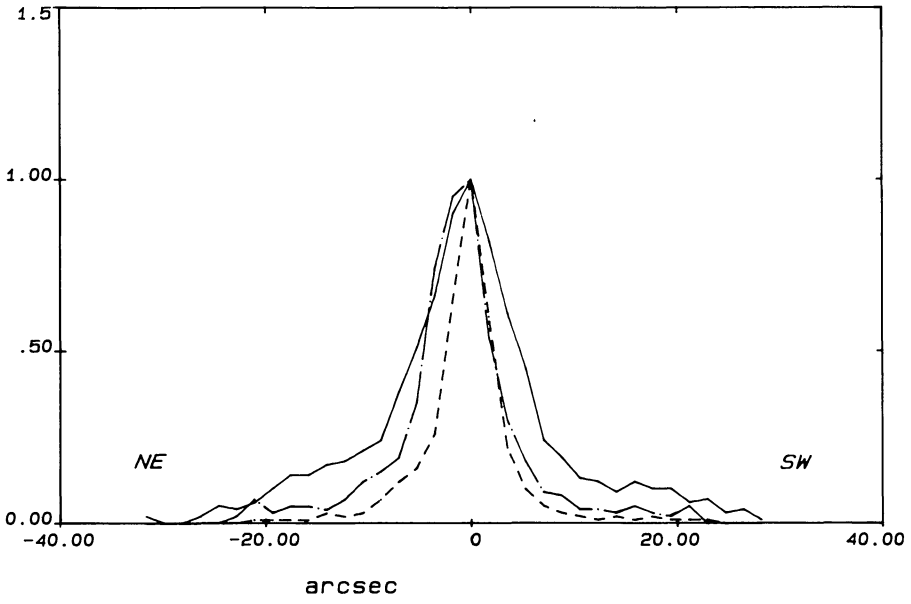

Fig. 3. Variation of the intensity of different emission lines along the IPCS slit ([O II] λ3727: solid line; Hβ: dot-dashed line; [O III] λ5007: dashed line). The values have been normalized to 1 in the point of maximum intensity

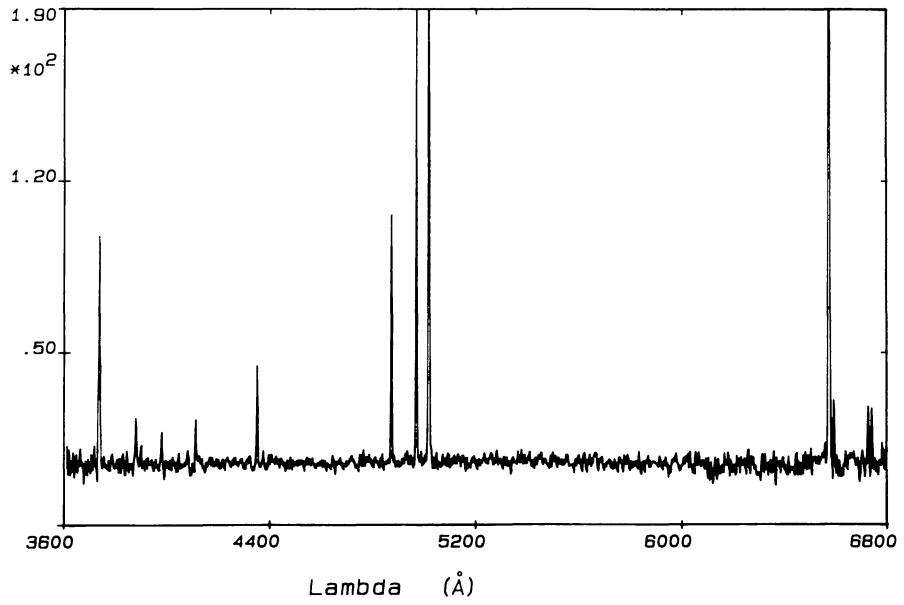

Fig. 4. Optical spectrum of NGC 5253. The units are 10^{-16} erg/cm^2 sÅ

The absolute intensity of Hβ corrected for interstellar absorption is lower than the values quoted by other authors (see Table 1). These differences are due to the smaller aperture employed in our observations. The equivalent width of Hβ (114 Å) refers of all the nucleus of the galaxy. However, a detailed examination of the variation of this quantity along the image shows that it reaches a maximum in the central 7″, corresponding to nucleus (a), where the value is $W(\mathrm{H}\beta) = 335 \pm 35$ Å. There are no references of $W(\mathrm{H}\beta)$ measured in previous works.

2.2. *Ultraviolet data*

We have searched the International Ultraviolet Explorer (IUE) archives in order to collect all the existing UV data of NGC 5253. There are a total of 17 images (9 SWP and 8 LWR), all of them taken with the large aperture and in the low-dispersion mode. Most of them show an underexposed continuum. There are only two images with a good exposure level: SWP 13484 and LWR 3131 (see Table 2).

The spectra have been extracted from the Extended Line-by-Line images, formed by 55 spatial increments corresponding each one to 1″.078 on the sky, by adding the central 30 scans and substracting a smoothed background. After that, they were calibrated in absolute energy units using the IUE sensitivity functions (Holm et al., 1982). The two selected spectra are shown in Fig. 5. A first inspection of the spectra show their similarity with those emitted by extragalactic H II regions (Rosa, 1980; Lequeux et al., 1981; Rosa et al., 1984) and star-burst galaxies (Weedman et al., 1981; Huchra et al., 1984). All the short-wavelength spectra (1150–1950 Å), despite the low exposition level of the continuum

Table 3. Emission lines intensities

Line	$I(\lambda)$	$F(\lambda)$	
3727 [O II]	125	192	a
3869 [Ne III]	26	38	b
3889 H8+He I	9	12	b
3968 [Ne III]+H7	17	23	b
4102 Hδ	17	22	b
4340 Hγ	39	47	b
4363 [O III]	6	7	c
4472 He I	4	5	c
4686 He II	< 1.4	< 1.5	c
4861 Hβ	100	100	a
4959 [O III]	159	155	a
5007 [O III]	461	438	a
5876 He I	10	7	c
6548 [N II]	11	7	b
6563 Hα	432	275	a
6584 [N II]	33	21	b
6678 He I	< 3	< 2	c
6717 [S II]	25	15	b
6731 [S II]	24	15	b
$E(B-V)$	0.41		
$F(H\beta)$	2.17 10^{-13} erg/cm^2 s (corrected for $E(B-V)=0.41$)		
$W(H\beta)$	114 ± 8 Å		

The fourth column representes an estimate of the error in the line intensity measurement: (a) error <10%; (b) 10% < error < 20%; (c) error > 20%.

The Hβ flux and equivalent width correspond to an aperture of 0".4 × 1'

Table 4. Ultraviolet absorption lines

λ_{obs}	Ident.	Origin	Ref.
1175	C III	Maximun in B1	4
1256–1262	Fe V	O3–O7	4
	Si II	B1–B9	4
	S II	Interstellar	2
1303–1308	Si III	Maximun in O3	4
	Si II	B2–B8	4
	O I + Si II	Interstellar	2
1335–1338	C II	B8 + Interstellar	2, 4
1394–1404	Si IV	Maximun in B1	4
1528	Si IV	Interstellar	1, 2
1548–1550	C IV	O – B	1
1608–1614	Fe II	Interstellar	1
1674	Al II	Interstellar	3
1854–1864	Al III	Interstellar	2
2382	Fe II	Interstellar	1
2599	Fe II	Interstellar	1
2803	Mg II	Interstellar	1
2852	Mg I	Interstellar	1

References: 1) Rosa (1980); 2) Rosa et al. (1984); 3) Lamb et al. (1984); 4) Heck et al. (1984)

in most of them, exhibits similar features: a blue continuum that rises towards shorter wavelengths, indicating the existence of very blue stars, and several absorption lines, while its relative flatness is indicative of a large amount of extinction. However, the absence of a strong 2200 Å feature suggests that the reddening law must be different from the galactic one. Only one emission, C III] λ1909 of nebular origin, can be certainly identified (At low densities, as in this case, the component of the doblet at 1907 Å dominates over the component at 1909 Å). Its presence indicates, according to Stasinska (1982), that the ionizing stars have a high effective temperature, $T_{eff} \sim 45000$ K. It is noteworthy that this line only appears in 12 of the extragalactic H II regions of Rosa et al. (1984) Catalog.

Table 4 presents the possible identifications for the absorption lines found. In somes cases a weak emission component in the red side of the Si IV and C IV lines can be noticed in the spectra of NGC5253. An examination of the IUE Low Dispersion Atlas (Heck et al., 1984) shows that these lines are stronger in supergiants, having strong P Cygni profiles in this type of stars. The velocities of the centers of the blue-shifted absorptions in NGC5253 are, after correcting for the celocity of the galaxy, ~ -1700 and ~ -1300 km s^{-1} for Si IV and C IV respectively, values typical of O stars and similar to those found by Rosa (1980) in NGC604.

The long-wavelength spectrum (1900–3200 Å) shows a much lower signal-to-noise ratio. All the absorption lines present are of interstellar origin. The most remarkable feature is a weak emission that can be identified as C II] λ2326. The photoionization models of Stansinska (1982) indicates that this line, as in the case of C III] λ1909 is a sign of high effective temperatures. Other features appearing near 1536, 1830 and 2200 Å are instrumental artifacts.

The IUE spatial resolution depends strongly on the focusing conditions. In the optimum case the smallest values are 4".6 at 1350 Å and 4".2 at 2900 Å for the SWP and LWR cameras respectively (Cassatella et al., 1985). In Fig. 2, the solid line shows the profile of the continuum between 1300 and 1400 Å along the slit. As in the case of the optical continuum there is a second concentration at ~6" SW the first one, corresponding to nucleus (b). In the ultraviolet is much more pronounced, which is more likely a consequence of the different position angle.

A detailed knowledge of the extinction law is necessary in order to study the ultraviolet spectra of extragalactic H II regions (see Lequeux et al., 1981). We have corrected the spectrum of NGC5253 in the following way: first, we have used the galactic mean extinction law (Savage and Mathis, 1977) along with the color excess $E(B-V)=0.04$, as derived from H I maps. The nucleus of NGC5253 being a metal-poor region, the LMC extinction law (Nandy et al., 1980) has been used to correct for the remaining extinction ($E(B-V)=0.37$).

Table 5 shows the observed and corrected intensities of the emission lines present in the ultraviolet spectrum.

3. Physical conditions and chemical composition

3.1. *Electron temperature and density*

The same atomic data as in Zamorano and Rego (1985) have been used to derive the electron temperature T_e, density and chemical abundances.

From the [O III] $\lambda\lambda$4959, 5007/λ4363 lines intensity ratio we find T_e(O III) = 15400 ± 1400 K, where the error corresponds to an uncertainty of 20% in the λ4363 line.

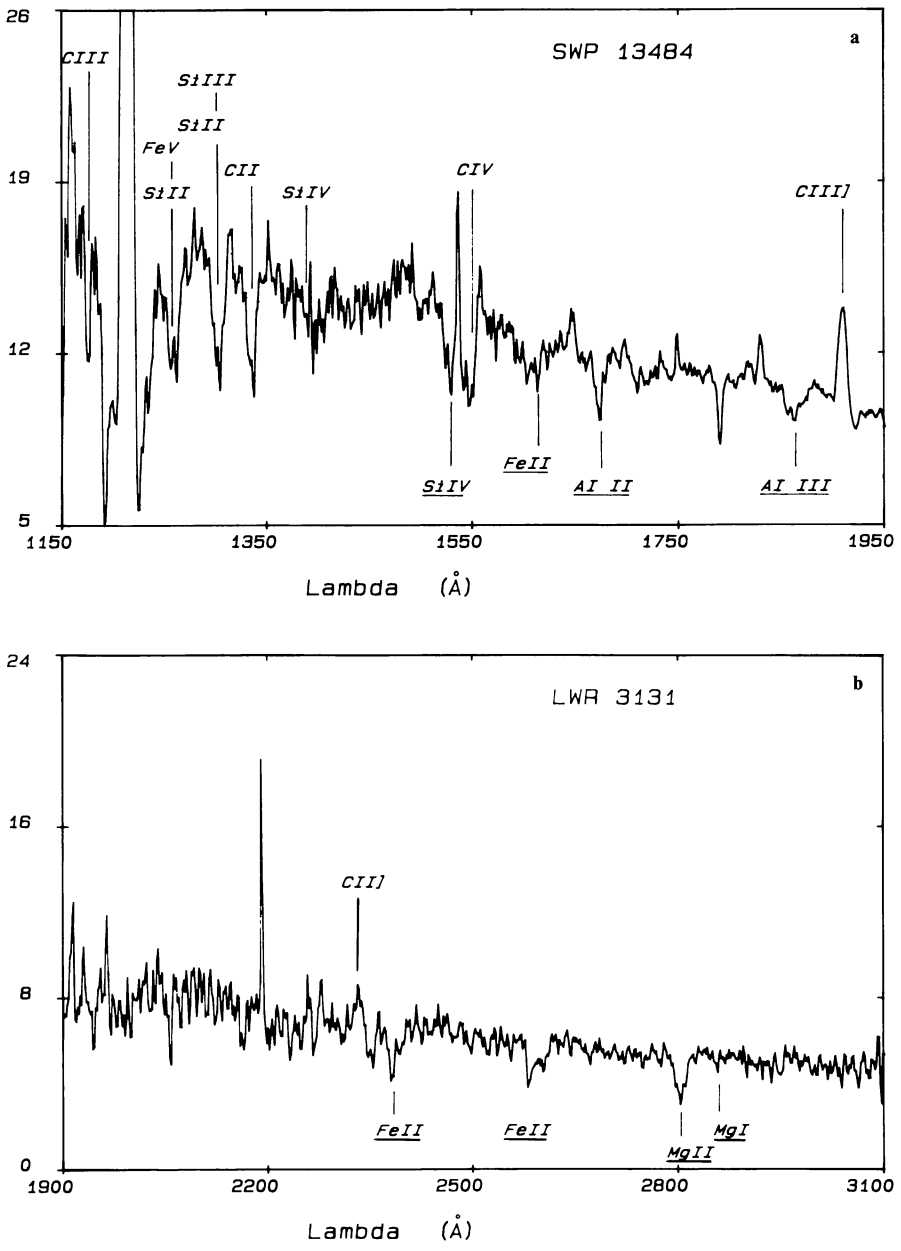

Fig. 5. **a** Short and **b** long wavelength IUE spectra of NGC5253. The most prominent stellar absorption and nebular emission lines are identified. The units are 10^{-14} erg/cm^2 s Å. The emissions near 1536, 1830, and 2200 Å are instrumental artifacts. Lines underlined are of interstellar origin. The anormal strength of these lines in the long-wavelength spectrum suggests that they are mainly formed in NGC5253

Table 5. Ultraviolet emission lines

Line	$I(\lambda)$	$F(\lambda)$
1909 C III]	$5.2\ 10^{-13}$	$1.1\ 10^{-9}$
2326 C II]	$3.6\ 10^{-13}$	$3.7\ 10^{-9}$

In units of erg/cm^2 s.

$F(\lambda)$ is the intensity corrected for interstellar absorption with $E(B-V)=0.41$ (see text)

The electron density derived from the [S II] $\lambda\lambda$6717/6731 ratio is 160 cm^{-3}.

3.2. *Chemical abundances*

The ionic abundances have been derived assuming T_e(O III) to be representative for the whole emission region. Fits from Zamorano and Rego (1985) for the line emissivities have been used.

The total O, N, Ne, and S abundances were obtained from the expresions:

$$\frac{O}{H}=\frac{O^+}{H^+}+\frac{O^{2+}}{H^+}, \quad (1)$$

$$\frac{N}{H}=\frac{N^+}{H^+}\frac{(O^+ + O^{2+})}{O^+}, \quad (2)$$

Table 6. Ionic and total abundances

	$N(X)/N(H)$	$12+\log N(X)/N(H)$
Ion		
He^+	0.087	10.94
O^+	$1.2\ 10^{-5}$	7.08
O^{2+}	$3.5\ 10^{-5}$	7.56
N^+	$1.3\ 10^{-6}$	6.10
S^+	$3.4\ 10^{-7}$	5.53
Ne^{2+}	$1.5\ 10^{-5}$	7.19
Element		
He	>0.087	>10.94
O	$4.8\ 10^{-5}$	7.68
N	$4.8\ 10^{-6}$	6.68
S	$1.2\ 10^{-6}$	6.10
Ne	$2.2\ 10^{-5}$	7.34

$$\frac{Ne}{H}=\frac{Ne^{2+}}{H^+}\frac{(O^+ + O^{2+})}{(O^{2+}-0.2\,O^+)}, \tag{3}$$

$$\frac{S}{H}=\frac{S^+}{H^+}\frac{(0.25\,(O^+ + O^{2+}))}{(O^+)}, \tag{4}$$

based on Stasinska (1982) models, and are presented in Table 6.

The He^+/H^+ abundance has been derived from the intensities of the three HeI lines present. From the computations of Brocklehurst (1971, 1972) for $T_e = 15400$ K, we obtain a weighted mean of $y^+ = 0.087$. No attempt has been made to correct for self-absorption effects. The He^{2+}/H^+ abundance could not be obtained due to the absence of the He II λ4686 line in the spectra of NGC5253. The total Helium abundance $y = y^0 + y^+ + y^{2+}$ must be higher than the y^+ value obtained, resulting in a mass abundance $Y > 0.258$.

The errors in the computed abundances arise from the uncertainty in the line intensities and from the error in the electron temperature. Our computations show that, with an uncertainty in T_e of $\sim$1400 K (see above), and the errors in the line intensities given in Table 3, the abundances of elements collisionally excited have a mean error of $\sim$40%. In the case of Helium it is slightly lower ($\sim$35%), and it is due mainly to the error in the measurement of the lines.

The photoionisation models of Stasińska (1980) suggests that for the metallicity and electron temperature derived, we would require $T_{\rm eff} \sim 45000$ K for the ionizing radiation.

4. Models

4.1. Description of the models

In order to study the characteristics of the star formation processes in extragalactic H II regions we have computed a set of models to follow the evolution of a cluster of young stars.

As imput data for the energy distribution of the stars we have used Kurucz's stellar atmosphere models (1979) of solar abundance. The evolution of the stars in the cluster has been computed according to the following evolutive tracks:

a) For $M = 1.1$, 1.4, and $1.75\,M_\odot$, evolutive tracks from Mengel et al. (1979) have been used.

b) For $M = 2$,3, and $5\,M_\odot$, we have used models by Alcock and Paczyński (1978).

For larger masses all the evolutive tracks have been taken from models by Maeder, in order to work with a homogeneous set of data.

c) Models for $M = 9$, 15, and $30\,M_\odot$ have been taken from Maeder (1981b); $M = 60\,M_\odot$ from Maeder (1981a), both of these with an intermediate mass loss rate (case B).

d) The evolution of a $120\,M_\odot$ star has been taken from Maeder (1980). The mass loss parametrization chosen corresponds to what this author calls $K = 2\,K$(BC) (intermediate case).

The use of newer models computed by the same author (Maeder, 1983) does not lead to significant changes in our results.

All the evolutive tracks used correspond to a solar composition ($X = 0.70$, $Y = 0.27$). In the case of Mengel et al. models the values have been interpolated to this abundance.

We have assumed that all the stars of the cluster are formed simultaneously, with an Initial Mass Function (IMF) of the form:

$$\phi(m) = \phi_0\, m^{-\alpha}\,\mathrm{dm} \tag{5}$$

being ϕ_0 a normalization factor computed from the expression:

$$\int_{M_{\rm low}}^{M_{\rm up}} \phi(m)\,\mathrm{dm} = 1. \tag{6}$$

The value of $M_{\rm low}$ has been fixed in all the models to $0.07\,M_\odot$. The upper mass limit will be allowed to vary from model to model.

If $M_{\rm gas}$ is the mass of gas transformed in stars during the burst, then the number of stars formed with mass $m(i)$ is given by:

$$N(m(i)) = M_{\rm gas} \int_{m_2}^{m_1} \phi(m)\,\mathrm{dm} \tag{7}$$

being $m(i)$ the masses for which evolutive tracks are available, and defining m_1 and m_2 as:

$$m_1 = \sqrt{m(i)\,m(i-1)}\,, \tag{8}$$

$$m_2 = \sqrt{m(i+1)\,m(i)} \tag{9}$$

following the formulation of Bruzual (1983).

In a given instant the total luminosity emitted by the cluster at the wavelength λ is:

$$L_\lambda = \sum_i N(m(i))\,L_\lambda(i). \tag{10}$$

The emission of each star is computed taking its effective temperature and luminosity from the evolutive tracks, computing its surface gravity

$$\log\left(\frac{R(i)}{R_\odot}\right) = 0.5\log\left(\frac{L(i)}{L_\odot}\right) - 2\log\left(\frac{T_{\rm eff}(i)}{10^4}\right) - 0.473, \tag{11}$$

$$\log(g(i)) = \log(g_\odot) + \log\left(\frac{m(i)}{M_\odot}\right) - 2\log\left(\frac{R(i)}{R_\odot}\right), \tag{12}$$

and entering with the values of $T_{\rm eff}$ and $\log(g)$ in Kurucz's models. Finally the luminosity emitted by the star is simply:

$$L_\lambda(i) = 4\pi\,R(i)^2\,F_\lambda(i)\,. \tag{13}$$

This procedure has been followed for a total of 14 points from 1000 to 7500 Å in intervals of 500 Å.

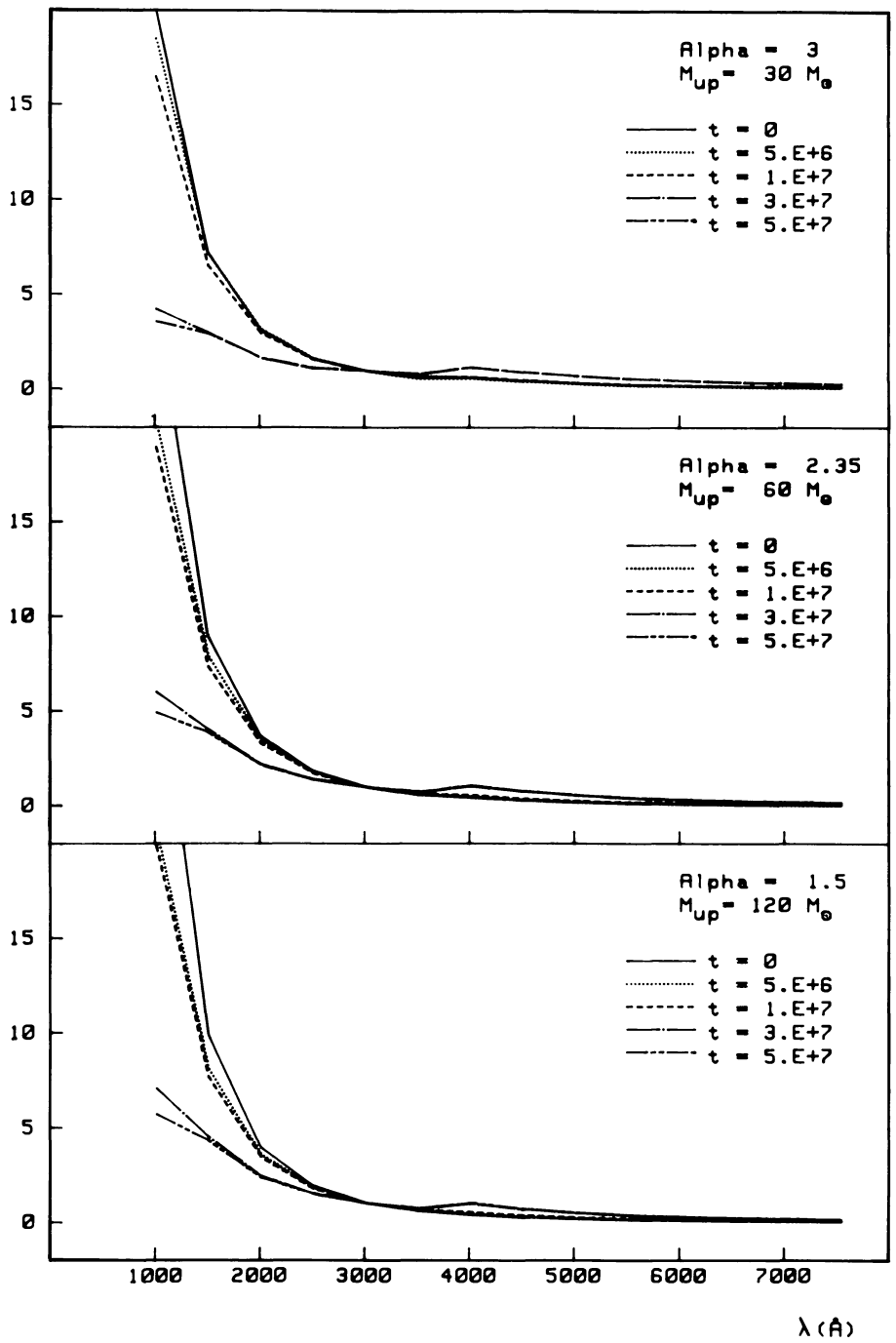

Fig. 6. Some examples of the computed models. The figure shows the evolution of the continuum radiation emitted by a cluster of young stars formed in an instantaneous burst. The shown models are: a) $\alpha = 3$; $M_{up} = 30\,M_{\odot}$, b) $\alpha = 2.35$; $M_{up} = 60\,M_{\odot}$, c) $\alpha = 1.5$; $M_{up} = 120\,M_{\odot}$. All models have been normalized to $L(3000\,\text{Å}) = 1$ for a better comparison. The first model represents an extreme case without very massive stars and with a steep IMF. The last one represents the opposite situation: a flat IMF with high-mass stars

In the same way we have computed for each model the number of photons emitted in the Lyman continuum ($\lambda > 912$ Å) and the equivalent width of the line Hβ:

$$W(\mathrm{H}\beta) = 4.78\ 10^{-13}\ \frac{N_{\mathrm{Lyman}}}{L(4862\,\text{Å})}. \qquad (14)$$

The gas contribution to the observed continuum has been estimated using the expression:

$$L(\mathrm{gas}) = (\gamma(2q) + \gamma(\mathrm{H}^{+}) + \gamma(\mathrm{He}^{+}))\left(\frac{x(\mathrm{He}^{+})}{x(\mathrm{H}^{+})}\right)\frac{N_{\mathrm{Lyman}}}{\alpha_{\mathrm{B}}}. \qquad (15)$$

The expression has been evaluated for $X = 0.9$ and $x(\mathrm{He}^{+})/x(\mathrm{H}^{+}) = 0.13$.

We present out results for a total of nine models. They correspond to three different values of the slope of the IMF: a mass function rich in massive stars ($\alpha = 1.5$), for Salpeter's value for the solar neighbourghood ($\alpha = 2.35$), and for a distribution richer in low-mass stars ($\alpha = 3$).

Three values of the upper mass limit have been used for each case: 30, 60 and $120\,M_{\odot}$. Figure 6 shows the evolution of the continuum emission of the cluster for the nine models at five different ages: 0, $5\ 10^{6}$, 10^{7} $3\ 10^{7}$, and $5\ 10^{7}$ yr. For a better comparison the values have been normalized to $L(3000\,\text{Å}) = 1$.

Table 7. Evolution of the luminosity at 3000 Å

		t				
α	M_{up}	0	5	10	30	50
1.50	30	35.3	69.5	28.5	1.33	1.52
	60	87.2	111	28.0	1.31	1.49
	120	181	112	27.8	1.30	1.48
2.35	30	0.88	1.52	0.89	0.11	0.12
	60	1.45	2.08	0.89	0.11	0.12
	120	2.03	2.09	0.89	0.11	0.12
3.00	30	0.05	0.07	0.05	0.01	0.02
	60	0.06	0.08	0.05	0.01	0.02
	120	0.07	0.08	0.05	0.01	0.02

L(3000 Å) in units of 10^{31} erg/s $M_\odot$
t in units of 10^6 yr
M_{up} in solar masses

Table 9. Evolution of α_{uv}

		t				
α	M_{up}	0	5	10	30	50
1.50	30	3.15	3.01	2.94	2.18	2.10
	60	3.24	3.02	2.94	2.18	2.10
	120	3.31	3.02	2.94	2.18	2.10
2.35	30	3.09	2.98	2.89	2.01	1.95
	60	3.16	2.99	2.89	2.01	1.95
	120	3.22	2.99	2.89	2.01	1.95
3.00	30	2.85	2.84	2.71	1.58	1.56
	60	2.96	2.88	2.71	1.58	1.56
	120	3.01	2.88	2.71	1.58	1.56

t in units of 10^6 yr
M_{up} in solar masses

Table 7 presents the luminosity at 3000 Å in the nine models at the five ages above mentioned. The units are erg/s/solar mass of stars formed.

The behaviour of the equivalent width of Hβ for ages comprised between 0 and 10^7 yr is presented in Table 8 and Fig. 8.

In order to have a more qualitative formation of the evolution of the shape of the UV continuum we have computed an index defined as:

$$\alpha_{uv} = \left(\frac{\log F(1500\,\text{Å}) - \log F(3000\,\text{Å})}{\log(3000) - \log(5000)}\right). \quad (16)$$

The higher the value of α_{uv}, the higher is the slope of the UV spectrum. Table 9 shows the values of α_{uv} at different ages from 0 to 10^7 yr.

Finally we have computed a third parameter that we have called A, defined as:

$$A = \log\left(\frac{N_{Lyman}}{L(1500\,\text{Å})}\right), \quad (17)$$

where N_{Lyman} is the number of Lyman photons and L(1500 Å) the luminosity at 1500 Å.

This quantity is similar to the R defined by Tarrab (1985). This parameter is very useful to discriminate between models because, as this author states, the number of Lyman photons emitted by the cluster decreases much faster than the UV luminosity. Essentially, it gives the relation between the number of stars with $m > 20\,M_\odot$, responsible for the gas ionization, and stars with $m = 20\,M_\odot$, that are the main contributors to the emission at 1500 Å. The evolution of this parameter is presented in Table 10.

4.2. *Discussion of the models*

The variation of the shape of the continuum with age depends strongly on the slope of the IMF. For the three values of studied in this work, the UV spectrum shows a noticeable flattening after 10 millions years, due to the death of stars with masses greater than $9\,M_\odot$. The other remarkable feature is the increase of the

Table 8. Evolution of W(Hβ) (Å)

		t										
α	M_{up}	0	1	2	3	4	5	6	7	8	9	10
1.50	30	304	288	272	226	182	88	33	18	16	11	3
	60	564	508	433	255	44	88	33	18	16	11	3
	120	675	607	478	271	44	88	33	18	16	11	3
2.35	30	208	201	193	164	137	70	29	13	12	9	3
	60	413	380	335	215	56	70	29	13	12	9	3
	120	508	466	386	236	56	70	29	13	12	9	3
3.00	30	98	97	96	84	74	41	19	7	6	5	2
	60	203	193	179	129	51	41	19	7	6	5	2
	120	253	241	214	148	51	41	19	7	6	5	2

t in units of 10^6 yr
M_{up} in solar masses

Table 10. Evolution of A

α	M_{up}	t		
		0	5	10
1.50	30	13.45	12.92	11.45
	60	13.75	12.72	11.46
	120	13.27	12.71	11.46
2.35	30	13.27	12.79	11.40
	60	13.56	12.66	11.40
	120	13.60	12.65	11.40
3.00	30	12.92	12.51	11.34
	60	13.25	12.57	11.34
	120	13.41	12.57	11.34

t in units of 10^6 yr
M_{up} in solar masses

luminosity between 3500 and 4000 Å. This effect is caused by the contribution of cool stars, in whose spectrum there is a concentration of lines shortwards 4000 Å, and appears after 10^7 yr in the models with $\alpha = 1.5$ and 2.35, and after $5\ 10^7$ yr when $\alpha = 3$.

The equivalent width of Hβ has already been described as a powerful age indicator by numerous authors. Our results show that it is very sensitive to M_{up} for ages less than $4\ 10^5$ yr. After that, its value is so low that it cannot be used to discriminate between different mass functions. For a given upper mass limit it is also a good indicator of the IMF slope in the early stages of the H II region evolution. It is worthwhile to note the importance of the nebular continuum contribution when computing the Hβ equivalent width. Our results show that in the most extreme cases (e.g. $\alpha = 1.5$, $M_{up} = 120\ M_\odot$) it can be almost as important as the stellar continuum emission. Thus, much higher values of W(Hβ) would be found when neglecting this term, leading to an overestimate of the age. The UV continuum shape does not depend on the upper mass limit for ages greater than 10^7 yr, although it is particularly sensitive to this parameter for smaller ages ($t < 5\ 10^6$ yr). However, it is useful in discriminating between different IMF specially after 10 millions yr.

The index A decreases considerably in the first 10^7 yr. After this age it becomes insensitive both to M_{up} and α. In the first stages it can be a good discriminator between different upper mass limits.

5. Discussion

In this section we will limit the discussion to the innermost part of the nucleus of NGC5253, i.e. nucleus (a), responsible for the strongest emission, and therefore the site of the most intense star formation activity. The linear diameter of this region is about 140 pc, consistent with the mean value of a "star forming cell", as defined by Hunter (1982). Probably this region coincides with the IR source detected at 10 μ by Rieke (1976), whose diameter is less than 6″. We will use the thre age indicators defined in the previous section: W(Hβ), α_{uv} and A. The value of W(Hβ) in the central 7″ is 335 ± 35 Å (see Sect. 2.1). The slope of the UV continuum, corrected for extinction in our Galaxy is 1.26. Looking at Tables 8 and 9, it can be seen that this value is not consistent with the measured W(Hβ), that indicates a much lower age. After correcting the spectrum with $E(B-V) = 0.37$ using the large Magellanic Cloud (LMC) extinction law, it rises up to 4.01. We are now in the opposite case, this value being higher than that predicted by our models. Thuan (1986) has pointed out the existence of this problem: when trying to fit the UV spectrum to a theoretical model, sometimes the extinction required is lower than the obtained from the Balmer decrement. The effect is analogous to that found in the extinction derived from radio measurements, which generally is higher than that computed from optical data. This is obviously a geometrical effect, for, at each wavelength range, we observe the brightest regions, that are less affected by extinction, which is strongly wavelength dependent.

The number of Lyman photons emitted by the H II region is needed in order to compute the index A. We have assumed that all the observed radio emission is thermal (there is no evidence of a non-thermal contribution). Using the expresion given by Lequeux (1980):

$$N_{Lyman} = 7.53\ 1045\ S_\nu\,(\mathrm{Jy})\ \nu^{0.1}\ (T_e/10^4)^{-0.47}\ D\,(\mathrm{kpc})^2\ \mathrm{phot/s} \quad (18)$$

and using the radio measurements quoted by Moorwood and Glass (1982) S_ν(5 GHz) = 0.075 Jy and the electron temperature of $T_e = 15400$ K previously found, we get:

$$N_{Lyman} = 5.48\ 10^{45}\ D\,(\mathrm{kpc})^2\ \mathrm{phot/s}. \quad (19)$$

The extinction corrected luminosity at 1500 Å is:

$$L\,(1500\ \text{Å}) = 3.82\ 10^{32}\ D\,(\mathrm{kpc})^2\ \mathrm{erg/s} \quad (20)$$

which leads to $A = 13.16$.

The value of W(Hβ) is the first parameter that is going to restrict the age of the region. From Table 8 and Fig. 7, it can be seen that models with $\alpha = 3$ always predict very low values of W(Hβ), due to the lower fraction of high-mass stars responsible for the ionization of the gas. The observed W(Hβ) cannot be explained even with the presence of 120 $M_\odot$ stars. With $\alpha = 2.35$ an upper mass limit of 60 or 120 $M_\odot$ is needed. In these cases the age is respectively 2 and 2.3 millions years. For a flatter mass function ($\alpha = 1.5$) only upper mass limit of 60 and 120 $M_\odot$ are consistent with the observe value, leading to ages of 2.5 ($M_{up} = 60\ M_\odot$) and 2.7 ($M_{up} = 120\ M_\odot$) millions years.

Figure 8 shows, in the (α_{uv}, A) plane the positions of the four possible models along with the observed value corrected for extinction as explained above. Also shown is the locus of the points obtained when correcting the observed spectrum with values of $E(B-V)_{NGC5253}$ from 0.00 to 0.50. The models with $\alpha = 1.5$ predict very high values of Lyman photons, and the one with $\alpha = 2.35$ and $M_{up} = 60\ M_\odot$, very low. The best fit correspond to the model with $\alpha = 2.35$, $M_{up} = 120\ M_\odot$ and $t = 2.3\ 10^6$ yr. The reddening correction needed is $E(B-V)_{NGC5253} = 0.25$, much lower than the measured from the Balmer decrement ($E(B-V) = 0.41$).

The assumption of the LMC extinction law for NGC5253 could be incorrect. We cannot exclude that the real extinction law in this galaxy is intermediate between the LMC and the galactic one. In this case the shape of the extinction curve at 2200 Å should be similar to that of the Magellanic Clouds, for no absorption is observed in the spectrum. Lequeux et al. (1981) have used this assumption to explain the observed spectra of several extragalactic H II regions. However, due to the low metallicity of the nucleus of NGC5253 an LMC-like extinction law is more appropriate than the galactic one.

Comparing the observed and predicted luminosity at 1500 Å, the mass of gas transformed in stars during the burst is

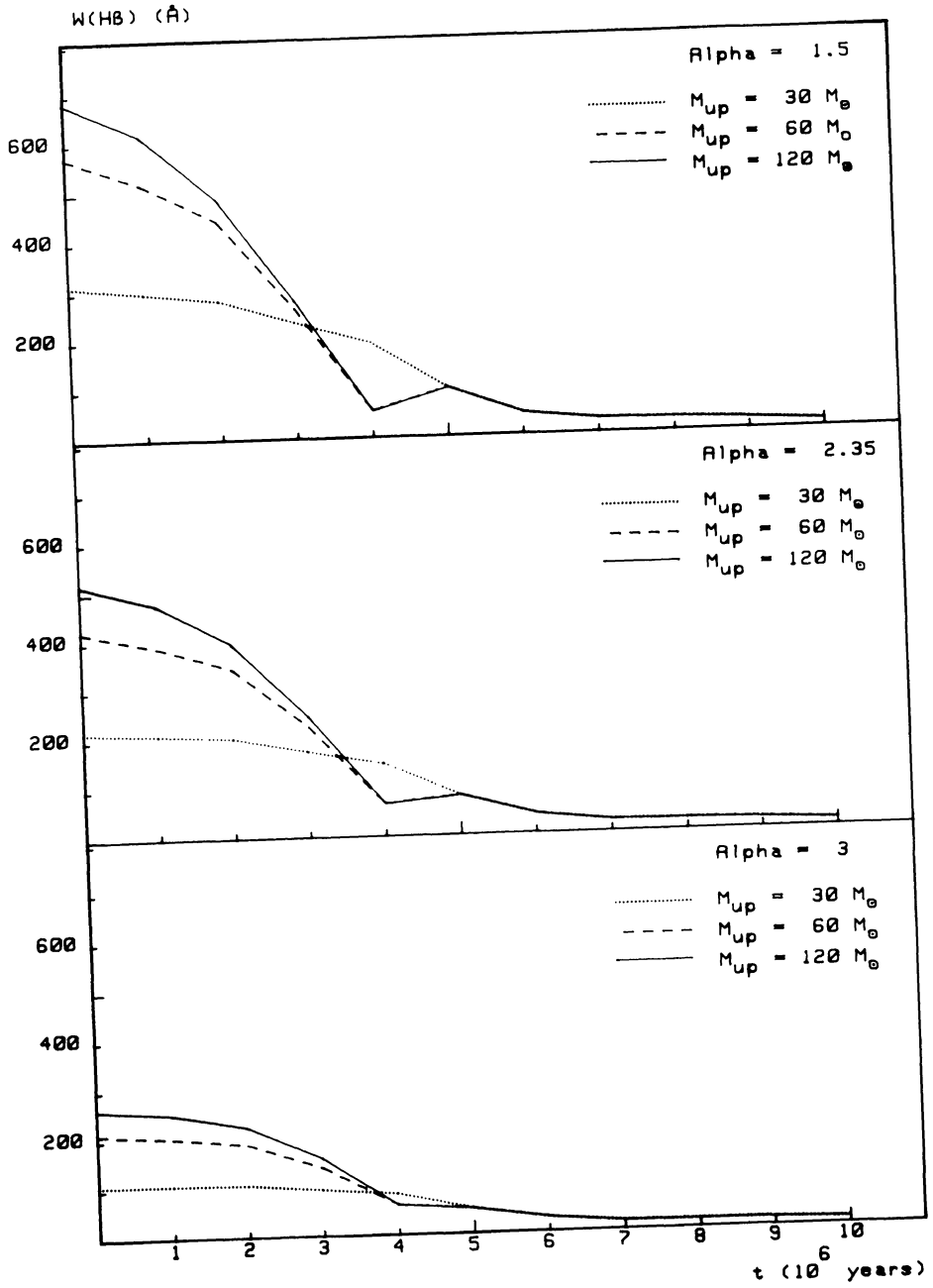

Fig. 7. Evolution of the equivalent width of Hβ for different values of the IMF slope and the upper mass limit

$M_{gas} = 1.8\ 10^5\ M_\odot$, assuming a distance of 4 Mpc. This leads to a total of $6.5\ 10^3$ O stars. The derived age is consistent with the results of Moorwood and Glass (1982). In this paper, based on IR photometry, a deficiency of giant and supergiant stars and supernovae remnants relative to ionizing stars is found when comparing NGC5253 to M 82. These authors estimate that the age is lower than 10^7 yr.

Lequeux et al. (1981) have computed the effective temperature and the mass of Oxygen ejected by a cluster of young stars as a function of the IMF slope and the age. For a model with $\alpha = 2.5$, $M_{up} = 110\ M_\odot$ and $t = 2\ 10^6$ yr the effective temperature is 37000 K, consistent with the value estimated from other considerations (see Sect. 3). Several authors (Durret et al., 1985; Melnick et al., 1985) have indicated that the values of Teff found from ionization degree considerations and evolutive models are different, the latter being smaller by ~15%, as in our case. As Oxygen is ejected into the interstellar medium only after $4\ 10^6$ yr, the gas in the nucleus of NGC5253 must have been enriched in previous bursts. The spectra of NGC5253 does not exhibit the typical features of Wolf-Rayet stars. Neither the UV emission lines nor the bump near 4686 Å are present. The weak P Cygni profile detected in the line C IV λ1550 can be easily accounted for by O supergiants. Evolutionary tracks from Maeder (1983) show that a $60\ M_\odot$ star reach the Wolf-Rayet stadium after $4.2\ 10^6$ yr. For higher masses stars with a high mass-loss rate evolve quickly to the left side of the HR diagram, becoming quasi-homogeneous. A star with an initial mass of $120\ M_\odot$ reaches the Wolf-Rayet phase ($Xs < 0.42$) after $2.8\ 10^6$ yr (Maeder, 1983). We can conclude that only a small fraction of the stars of the nucleus of NGC5253 have reached this state.

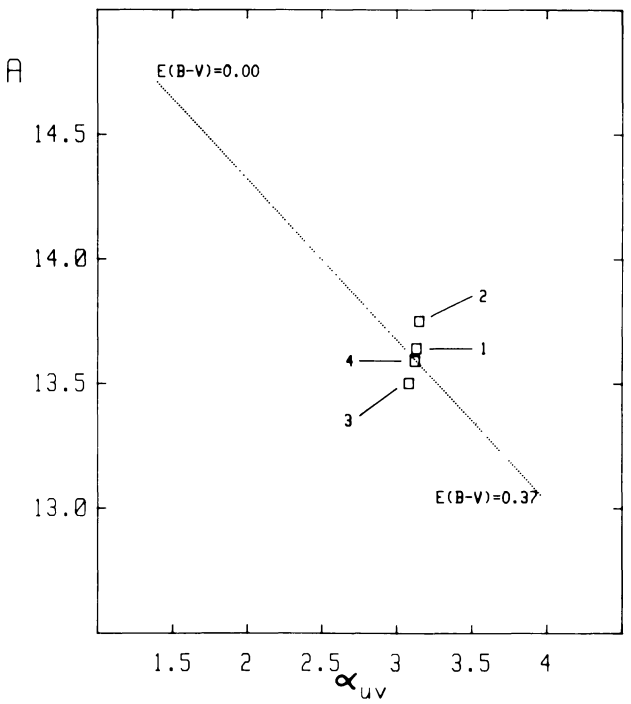

Fig. 8. Position of the different models for NGC5253 (a) according to the measured value of $W(H\beta)$ in the plane (α, A). The four possible models are: 1) $\alpha = 1.5$; $M_{up} = 60\,M_\odot$; $t = 2.5\ 10^6$ yr. 2) $\alpha = 1.5$; $M_{up} = 120\,M_\odot$; $t = 2.7\ 10^6$ yr. 3) $\alpha = 2.35$; $M_{up} = 60\,M_\odot$; $t = 2\ 10^6$ yr. 4) $\alpha = 2.35$; $M_{up} = 120\,M_\odot$; $t = 2.3\ 10^6$ yr. The line shows the effect of correcting the observed UV spectrum with values of $E(B-V)$ from 0 to 0.37 using the LMC extinction law

6. Conclusions

We have studied optical and ultraviolet spectra of the nucleus of NGC5253, in order to obtain information about the processes of star formation that are taking place in the innermost of this peculiar galaxy, which appears to be a typical starburst.

The optical spectra show a blue continuum and emission lines typical of extragalactic H II regions. The high electronic temperature is consistent with the low abundance of Oxygen, main coolant in this type of objects. The measured extinction is much higher than that derived from the Hydrogen maps of our Galaxy indicating than most of the observed reddening is produced in the observed galaxy. The ultraviolet data confirm the existence of massive stars with a high effective temperature ($T_{eff} = 45000$ K). The shape of the ultraviolet continuum indicates that, either the absorption in the UV is lower than in the visible, due to an obvious geometrical effect, or that the extinction law in this galaxy is intermediate between the galactic and the LMC one. In any case, the age of the brightest knot of the nucleus of NGC 5253 is less than three million yr. The slope of the IMF is either Salpeter's value or flatter, and the presence of stars with $m > 60\,M_\odot$ is necessary to explain the emitted Lyman luminosity.

Acknowledgements. We wish to thank Dr. W. Wamsteker for providing us with the IPCS observations of NGC5253, and for his useful remarks on the original manuscript.

References

Aitken, D.K., Roche, P.F., Phillips, M.M.: 1982, *Monthly Notices Roy. Astron. Soc.* **199**, 31
Alcock, C., Paczyński, B.: 1978, *Astrophys. J.* **223**, 244
Brocklehurst, M.: 1971, *Monthly Notices Roy. Astron. Soc.* **153**, 471
Brocklehurst, M.: 1972, *Monthly Notices Roy. Astron. Soc.* **157**, 211
Bohuski, T.J., Burbidge, E.M., Burbidge, G.R., Smith, M.G.: 1972, *Astrophys. J.* **175**, 329
Boksenberg, A.: 1972, in *ESO Workshop on Two Dimensional Photometry*, p. 295
Bottinelli, L., Gouguenheim, L., Heidmann, J.: 1972, *Astron. Astrophys.* **17**, 445
Bruzual, G.: 1983, *Astrophys. J.* **273**, 105
Burbidge, E.M., Burbidge, G.R.: 1962, *Astrophys. J.* **135**, 696
Burstein, D., Heiles, C.: 1984, *Astrophys. J. Suppl.* **54**, 33
Campbell, A., Terlevich, R.: 1984, *Monthly Notices Roy. Astron. Soc.* **211**, 15
Cassatella, A., Barbero, J., Benvenuti, P.: 1985, *Astron. Astrophys.* **144**, 335
De Vaucouleurs, G., de Vaucouleurs, A., Corwin, H.G.: 1976, "Second Reference Catalog of Bright Galaxies", Univ. of Texas Press
Durret, F., Bergeron, J., Boksemberg, A.: 1985, *Astron. Astrophys.* **143**, 347
Evans, D.: 1952, *The Observatory* **869**, 164
Gaposhkin, C.: 1936, *Astrophys. J.* **83**, 173
Heck, A., Egret, D., Jascheck, M., Jascheck, C.: 1984, "IUE Low Dispersion Spectra Reference Atlas. Part I: Normal Stars", ESA SP-1052
Holm, A., Bohlin, R.C., Cassatella, A., Ponz, D.P., Schiffer, F.H.: 1982, *Astron. Astrophys.* **122**, 341
Hubble, E., Lundmark, K.: 1923, *Publ. Astron. Soc. Pacific* **34**, 292
Huchra, J.P. et al.: 1983, *Astrophys. J.* **274**, 125
Hunter, D.: 1982, *Astrophys. J.* **260**, 81
Hunter, D., Gallagher, J., Rauntenkranz, D.: 1982, *Astrophys. J. Suppl.* **49**, 53
Kurucz, R.: 1979, *Astrophys. J. Suppl.* **40**, 1
Lamb, S., Gallagher, J.S., Hjellming, M.S., Hunter, D.A.: 1984, *Astrophys. J.* **291**, 63
Lequeux, J.: 1980, in *Star Formation*, eds. A. Maeder, L. Martinet, Geneva Observatory, Sauverny, p. 35
Lequeux, J., Maucherat-Joubert, M., Deharveng, J.M., Kunth, D.: 1981, *Astron. Astrophys.* **103**, 305
Lewis, B., Davis, R.: 1973, *Monthly Notices Roy. Astron. Soc.* **165**, 213
Maeder, A.: 1980, *Astron. Astrophys.* **92**, 101
Maeder, A.: 1981a, *Astron. Astrophys.* **99**, 97
Maeder, A.: 1981b, *Astron. Astrophys.* **102**, 401
Maeder, A.: 1983, *Astron. Astrophys.* **120**, 113
Melnick, J., Televich, R., Eggleton, P.P.: 1985, *Monthly Notices Roy. Astron. Soc.* **216**, 255
Mengel, J.G., Sweigart, A.V., Demarque, P., Gross, P.G.: 1979, *Astrophys. J. Suppl.* **40**, 733
Middelburg, F., Crane, P.: 1979, in *Image Processing in Astronomy*, eds. G. Sedmak, M. Cappaccioli, R.J. Allen, Osservatorio Astronomico di Trieste, p. 25
Moorwood, A., Glass, I.: 1982, *Astron. Astrophys.* **115**, 84
Nandy, K., Morgan, D.H., Willis, A.J., Wilson, R., Gondhalekar, P.M., Houziaux, L.: 1980, *Nature* **283**, 725

Oke, J.B.: 1974, *Astrophys. J. Suppl.* **27**, 21
Osmer, P.S., Smith, M.G., Weedmann, D.W.: 1974, *Astrophys. J.* **192**, 279
Osterbrock, D.E.: 1974, "Astrophysics of Gaseous Nebulae", Freeman, San Francisco
Reif, K., Mebold, U., Goss, W.M., Van Woerden, H., Siegman, B.: 1982, *Astron. Astrophys. Suppl.* **50**, 451
Rieke, G.H.: 1976, *Astrophys. J.* **206**, L15
Rosa, M.: 1980, *Astron. Astrophys.* **85**, 121
Rosa, M., Joubert, M., Benvenuti, P.: 1984, *Astron. Astrophys. Suppl.* **57**, 361
Sandage, A., Brucato, R.: 1979, *Astron. J.* **84**, 472
Sandage, A., Tamman, G.: 1981, A Revised Shapley-Ames Catalog of Bright Galaxies
Savage, B.D., Mathis, J.S.: 1977, *Ann. Rev. Astron. Astrophys.* **17**, 73
Sersic, J.L., Carranza, M., Pastoriza, M.: 1972, *Astrophys. Space Sci.* **19**, 469
Stasińska, G.: 1980, *Astron. Astrophys.* **66**, 257
Stasińska, G.: 1982, *Astron. Astrophys. Suppl.* **48**, 299
Tarrab, I.: 1985, *Astron. Astrophys.* **150**, 151
Terlevich, R., Melnick, J.: 1981, *Monthly Notices Roy. Astron. Soc.* **195**, 839
Thuan, T.X.: 1986, in *Star Forming Dwarf Galaxies and Related Objects*, Frontieres, Paris, p. 105
Van den Bergh, S.: 1972, *J. Roy. Astron. Soc. Canada* **66**, 122
Veron, M.P.: 1984, *Astron. Astrophys. Suppl.* **58**, 665
Weedmann, D., Feldman, F.R., Balzano, V.A., Ramsey, L.W., Sramek, R.A., Wu, C.: 1981, *Astrophys. J.* **248**, 105
Wegner, G.: 1979, *Astrophys. Space Sci.* **60**, 15
Welch, G.: 1970, *Astrophys. J.* **161**, 821
Welch, G., Wallerstein, G.: 1969, *Publ. Astron. Soc. Pacific* **81**, 23
Zamorano, J., Rego, M.: 1985, *Astron. Astrophys. Suppl.* **62**, 173